Mapping the neural systems driving breathing at the transition to unconsciousness

Jesus Pujol [a,b,*], Laura Blanco-Hinojo [a,b], Héctor Ortiz [c], Lluís Gallart [d,e], Luís Moltó [d], Gerard Martínez-Vilavella [a], Esther Vilà [d], Susana Pacreu [d], Irina Adalid [d], Joan Deus [a,f], Víctor Pérez-Sola [b,g], Juan Fernández-Candil [d]

[a] MRI Research Unit, Department of Radiology, Hospital del Mar, Passeig Marítim 25-29, Barcelona 08003, Spain
[b] Centro Investigación Biomédica en Red de Salud Mental, CIBERSAM G21, Barcelona, Spain
[c] Department of Project and Construction Engineering, Universitat Politècnica de Catalunya (UPC), Barcelona, Spain
[d] Department of Anesthesiology, Hospital del Mar-IMIM, Barcelona, Spain
[e] Department of Surgery, Universitat Autònoma de Barcelona, Barcelona, Spain
[f] Department of Psychobiology and Methodology in Health Sciences, Autonomous University of Barcelona, Barcelona, Spain
[g] Hospital del Mar- IMIM and Department of Psychiatry, Institute of Neuropsychiatry and Addictions, Autonomous University of Barcelona, Barcelona, Spain

ARTICLE INFO

ABSTRACT

After falling asleep, the brain needs to detach from waking activity and reorganize into a functionally distinct state. A functional MRI (fMRI) study has recently revealed that the transition to unconsciousness induced by propofol involves a global decline of brain activity followed by a transient reduction in cortico-subcortical coupling. We have analyzed the relationships between transitional brain activity and breathing changes as one example of a vital function that needs the brain to readapt. Thirty healthy participants were originally examined. The analysis involved the correlation between breathing and fMRI signal upon loss of consciousness. We proposed that a decrease in ventilation would be coupled to the initial decline in fMRI signal in brain areas relevant for modulating breathing in the awake state, and that the subsequent recovery would be coupled to fMRI signal in structures relevant for controlling breathing during the unconscious state. Results showed that a slight reduction in breathing from wakefulness to unconsciousness was distinctively associated with decreased activity in brain systems underlying different aspects of consciousness including the prefrontal cortex, the default mode network and somatosensory areas. Breathing recovery was distinctively coupled to activity in deep brain structures controlling basic behaviors such as the hypothalamus and amygdala. Activity in the brainstem, cerebellum and hippocampus was associated with breathing variations in both states. Therefore, our brain maps illustrate potential drives to breathe, unique to wakefulness, in the form of brain systems underlying cognitive awareness, self-awareness and sensory awareness, and to unconsciousness involving structures controlling instinctive and homeostatic behaviors.

1. Introduction

During the transition between wakefulness and sleep, the brain needs to adapt functionally to the new context so as to optimally regulate bodily functions. Loss of consciousness may naturally occur in the form of sleep or may be induced by hypnotic agents. Although falling asleep is apparently abrupt in both instances, the phenomenon is complex and requires a large-scale reorganization of brain activity (Ogilvie, 2001; Merica and Fortune, 2004; Tanabe et al., 2020; Pujol et al., 2021). We have recently characterized the transition to unconsciousness induced by a hypnotic agent with a temporal analysis of functional MRI (fMRI) signal (Pujol et al., 2021). A global decline in synchronized brain activity was observed immediately after loss of consciousness followed by a transient decrease in cortico-subcortical coupling that was restored during the unconscious state. We proposed that such cortico-subcortical decoupling and subsequent re-coupling might allow the brain to detach from waking activity and reorganize into a functionally distinct state.

One example of a vital function that needs the brain to functionally readapt during the transition between states of consciousness is breathing. Breathing is regulated at basic brain levels ensuring the adequate oxygen and carbon dioxide exchange during sleep (Smith and Lee-Chiong, 2008; Benarroch, 2019). Nevertheless, breath control is more

complex while awake, when a greater number of factors may influence respiratory rhythm and amplitude (Horner, 2009; Masaoka et al., 2014; Trinder et al., 2014). For example, a major source of tonic drive to respiratory motoneurons originates from the brainstem ascending arousal system that promotes wakefulness (Horner, 2009). The breathing pattern, however, is also sensitive to more specific variations in neural activity associated with both the automatic expression of emotions (e.g., laughing) and the volitional control of the motor cortex (e.g., speaking) (Masaoka et al., 2014; Evans, 2010). Breathing, therefore, is a common element of the varied behavioral repertory in the conscious state.

Such a waking stimulus to breathe is lost during the transition to unconsciousness, which characteristically presents a transitory reduction in pulmonary ventilation until the unconscious state is reorganized and breathing control fully recovered (Naifeh and Kamiya, 1981; Ogilvie et al., 1989; Worsnop et al., 1998; Edwards and White, 2011; Trinder et al., 2014). Reduction of the excitatory inputs combines with the increase in inhibitory γ-amino butyric acid (GABA) release, and both predispose susceptible individuals to hypoventilation and obstructive sleep apnea (Horner, 2009; Edwards and White, 2011). The inhibitory action and the risk of apnea are larger by the effect of hypnotic agents (Smith and Lee-Chiong, 2008).

In the present study, we have analyzed the coupling of breathing to brain activity following a loss of consciousness gently induced by the hypnotic agent propofol. Our aim was to illustrate how the brain reorganizes itself to control a basic behavior when moving between states of consciousness and to further characterize the neural drives to breathing. Our hypothesis was that the transient decrease in ventilation after losing consciousness would coincide with the initial fMRI signal decline observed in the synchronized cerebral cortex prior to the cortico-subcortical dissociation phenomenon. At the system level, the transit from stable to transitorily reduced pulmonary ventilation would be coupled to the fMRI signal decline in brain areas relevant for modulating breathing in the awake state, and the subsequent ventilation recovery would be coupled to an increased fMRI signal in structures involved in breathing control during the unconscious state.

2. Methods

2.1. Study participants

Thirty healthy right-handed participants were initially selected for the project. The current study was based on 19 subjects showing optimal fMRI and ventilation data. The group included 10 males and 9 females with a mean age of 27.9 years (SD: 6.3 years). The characteristics of the sample and participant selection were fully described in our previous report (Pujol et al., 2021). Participants were required to meet the criterion of the American Society of Anesthesiologists (ASA) physical status ASA I (healthy, non-smoking, no or minimal alcohol) (Mayhew et al., 2019) and to show normal physical and laboratory exams for eligibility.

The study was conducted in accordance with the guidelines of the Declaration of Helsinki. The protocol was approved by the Spanish Agency of Medicines and Medical Devices, AEMPS (reference 5NFNF6V55C) and by the Ethical Committee of Clinical Research of the Parc de Salut Mar of Barcelona (reference n° 2017–7165). Written informed consent was obtained from all participants.

2.2. Experimental procedure

2.2.1. Overview of the experimental design

Functional MRI was continuously acquired for a total of 15 min. In the initial 3-minute period no drug was administered. Subsequently, a continuous intravenous infusion of propofol commenced, which was steeply increased every 2 min until the participant lost consciousness. The dose of propofol was then adjusted (at the effect-site) and maintained constant with the aim of keeping a superficial level of unconsciousness during the rest of the fMRI acquisition with no return to consciousness at this stage of the study (participants underwent a second study phase testing other hypotheses).

2.2.2. Induced loss of consciousness with propofol

Our aim was to progressively sedate the participant until consciousness was lost within the fMRI acquisition window using a slow propofol administration regimen. At the attained sedation level, breathing is spontaneous with no need for tracheal intubation and the individual can be awakened with moderately intense stimulation. A behavioral reference indicating "loss of conscious control", as a surrogate of conventional loss of consciousness, was obtained within the constraints of the MRI environment by recording the moment the participants ceased to squeeze a soft pneumatic balloon with their right hand. Participants were instructed to repeatedly squeeze the balloon at a practiced rate of approximately one movement every 3 s (0.3 Hz) throughout the MRI while they were awake. The actual squeezing rate recorded prior to loss of conscious control showed a mean of 0.30 Hz (SD, 0.08 Hz) (Pujol et al., 2021).

Loss of conscious control was thus marked by the participants ceasing to move their right hand and served to direct the temporal analyses. We previously identified (Pujol et al., 2021) that the transitional fMRI signal events (i.e., initial signal fall followed by a transient reduction in cortico-subcortical coupling) began just after the participants stopped moving their hand in 9 cases (specifically after a mean of 2.9 s and SD of 3.9 s), and after a temporal lapse (mean, 61.0 s; SD, 25.1 s) in the remaining 10 participants. In no case were the fMRI signal changes evident before the participants ceased to move their hand. In the current evaluation, we analyzed the changes in pulmonary ventilation during the identified fMRI transitional events (see below).

2.2.3. Anesthetic technique

A target-controlled system (Base Primea Orchestra®, Fresenius Kabi, Brézins, France) was used for a continuous intravenous infusion of propofol individually programmed at a target plasma concentration of 3.5 mcg/mL based on the Schnider model (Schnider et al., 1999). Propofol target plasma concentration was steeply increased by 0.5 mcg/mL every 2 min until participants ceased to move their hand for at least 20 s. At this moment (20 s after loss of conscious control), propofol target-controlled infusion was targeted at the effect-site (brain) concentration currently estimated by the model. Pulse oximetry (SpO2) and expired capnography (Oral-Trac®, Salter Labs, Arvin CA) were used to continuously monitor respiratory function throughout the experiment for safety purposes. Heart rate, pulse oximetry and carbon dioxide measures were recorded every 10 s. Oxygen (2 L/min) was administered throughout the study (Pujol et al., 2021).

2.2.4. Continuous breathing recording

Respiration was recorded using a pneumatic sensor (Philips 3T Respiratory Sensor) softly held between the thorax and abdomen, and data logger developed in-house using Labview 8.0 software (National instruments corp. Austin, TX). The measures were registered in a text file with a 25 msec sampling period. As described by Birn et al. (2008), the amount of air inspired with each breath was estimated by computing the difference between the maximum and minimum sensor positions at the peaks of inspiration and expiration, respectively. This difference was divided by the respiration period (i.e., the time between the peaks of the respiration waveform) to consider changes in both the rate and depth of breathing. Such a respiration volume per time (RVT) quotient allowed us to estimate relative variations in pulmonary ventilation over time (Fig. 1). RVT was expressed as% change from a baseline period (i.e., 30 s preceding the transition to unconsciousness). RVT measures were downsampled by a factor of 80 (i.e., by averaging every 80 samples from the RVT time series) to match the sampling rate of the fMRI data (TR= 2 s), so they could be used as a regressor in the fMRI time series analysis.
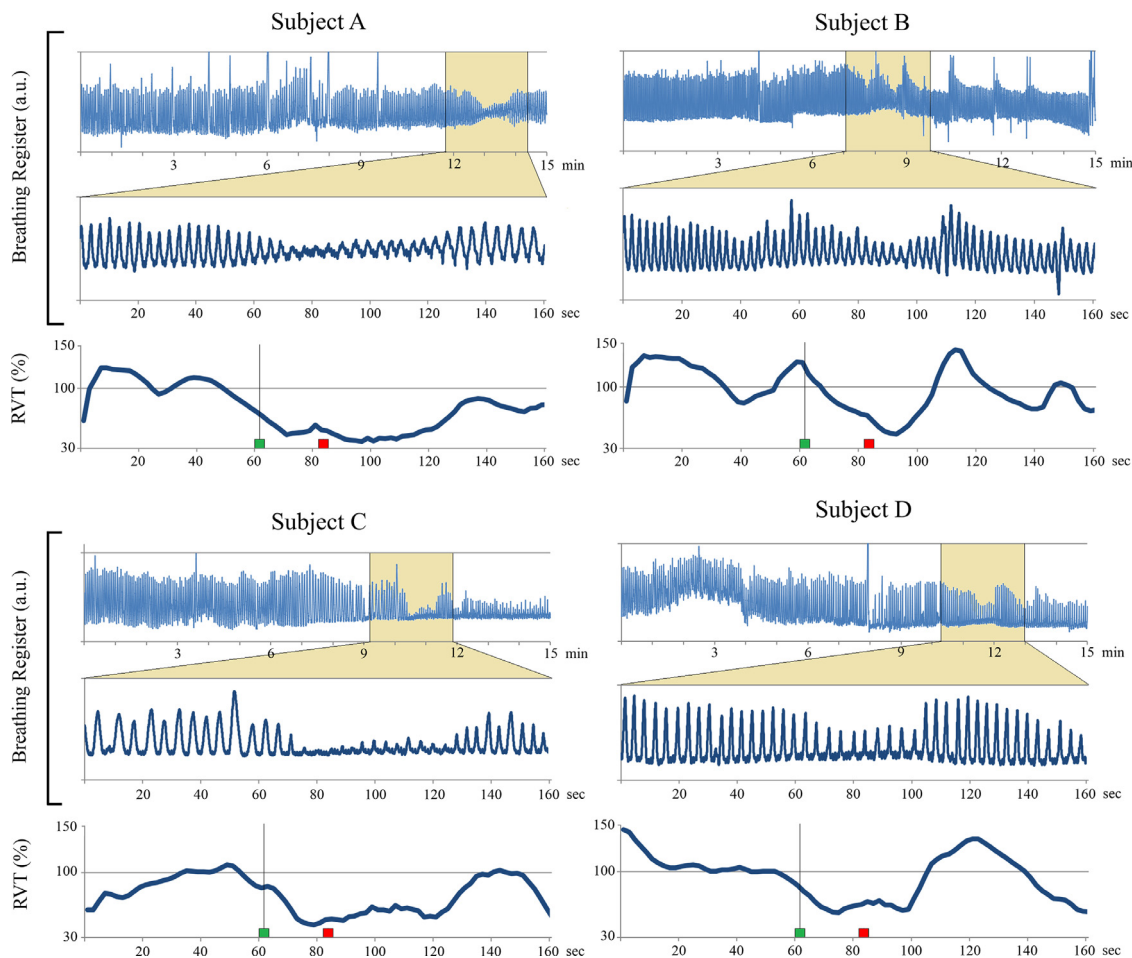
Fig. 1. Ventilation registers. The superior plots for each subject show the complete ventilation register (15 min) and the period selected for the analysis (2 min and 40 s). The red square indicates the reference point obtained in each subject from the fMRI signal time course of the cerebral cortex, which served to anchor signal oscillations and average out signal time courses across participants in the group analysis (Pujol et al., 2021). The green square and vertical bar indicate the group average onset of global decline in synchronized brain activity observed after loss of consciousness. The inferior plot for each subject shows the respiration volume per time (RVT) quotient estimated for each image acquisition volume (TR), expressed as% change from a baseline period (i.e., 30 s preceding the transition).

2.3. Functional MRI

2.3.1. MRI acquisition

A Philips Achieva 3.0 Tesla magnet (Philips Healthcare, Best, The Netherlands), equipped with an eight-channel phased-array head coil and single-shot echoplanar imaging (EPI) software, was used for the MRI assessment. The functional blood oxygen level–dependent (BOLD) sequence consisted of gradient recalled acquisition in the steady state (time of repetition [TR], 2000 ms; time of echo [TE], 35 ms; pulse angle, 70°) within a field of view of 240×240 mm, with a 64×64-pixel matrix, and a slice thickness of 4 mm (inter-slice gap, 0 mm) and acquisition voxel size of $3.75 \times 3.75 \times 4$ mm. A total of 34 interleaved slices were acquired to cover the whole-brain. Each functional time series consisted of 450 consecutive image sets or volumes obtained over 15 min.

2.3.2. MRI preprocessing

Imaging data were processed using MATLAB version 2016a (The MathWorks Inc, Natick, Mass) and Statistical Parametric Mapping software (SPM12; The Wellcome Department of Imaging Neuroscience, London). Preprocessing involved motion correction, spatial normalization and smoothing by means of a Gaussian filter (full-width half-maximum, 8 mm). Data were normalized to the standard SPM-EPI template and resliced to 3 mm isotropic resolution in Montreal Neurological Institute (MNI) space. Low-frequency fMRI signal drifts were removed using a

temporal high-pass filter with a cutoff of 128 s. No low-pass filter was applied.

All image sequences were inspected for potential acquisition and normalization artifacts. At this stage, 9 participants were removed from the initial 30-subject sample as a result of large head displacements preventing adequate image preprocessing or motion artifacts affecting the analyzed image volumes. Two additional participants were excluded due to technical issues in ventilation data registration. Therefore, 19 participants were valid for the analysis after careful selection.

2.3.3. Functional MRI analysis

To analyze the relationships between breathing variations and fMRI signal evolution during the transition to unconsciousness, a total of 80 fMRI volumes (2 min and 40 s) were used in each case that included the entire 100-s period encompassing the transitional fMRI signal events described in our early report and 60 s preceding the phenomenon. This transitional period was selected on an individual basis using a common point identified in the evolution of the cerebral cortex fMRI signal. Specifically, the common point for valid cases was the point at which the synchronized fMRI signal in the cortex passed from negative to positive values (Pujol et al., 2021). This benchmark, therefore, served to anchor signal oscillations and average out signal time courses across participants for an optimal group analysis.

SPM maps were generated using individual breathing (RVT) time courses as regressors in the first-level design matrices that also included
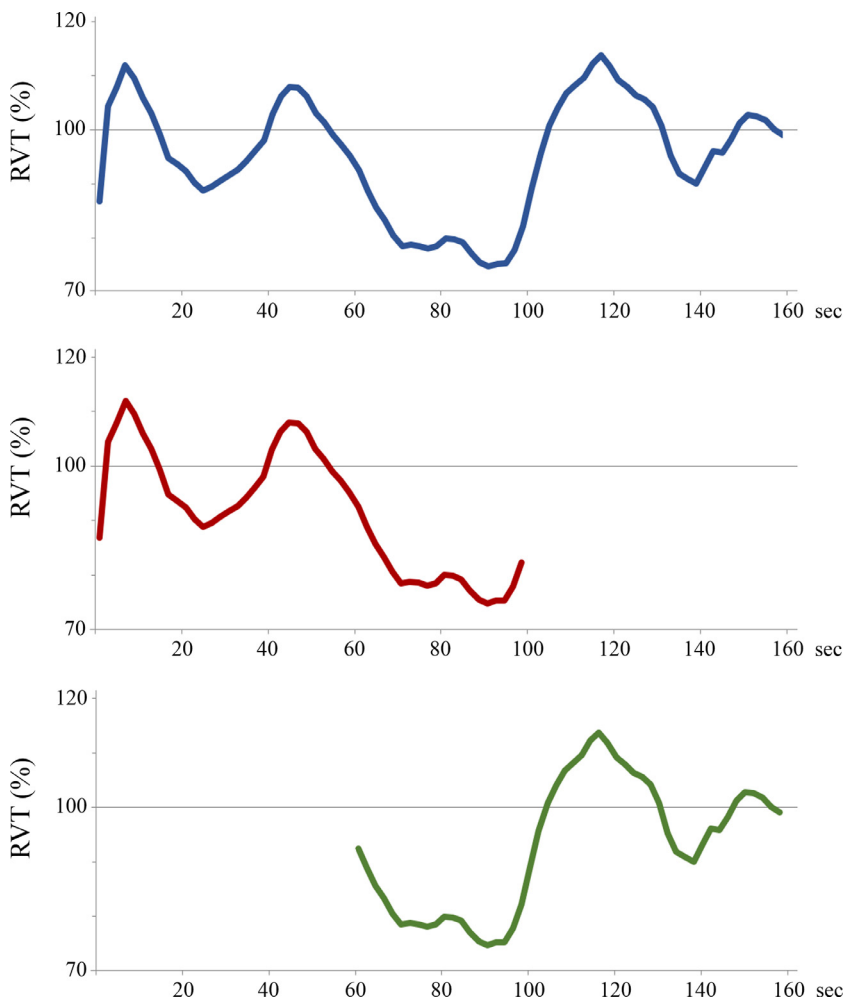
Fig. 2. Group average breathing measures. The superior plot shows the respiration volume per time (RVT) quotient estimated for each image acquisition volume (TR). The middle plot shows the selected "breathing-fall" 100-s period. The inferior plot shows the selected "breathing-recovery" 100-s period.

six motion estimates as co-variables and removal of volumes with interframe motion > 0.3 mm (Power et al., 2014). A delay of 4 s was applied to the regressor to adjust for the hemodynamic response latency (Poldrack et al. 2011; Khosla et al. 2021). No global MRI signal measures were used as nuisance regressors. This voxel-wise analysis, therefore, estimates the extent to which breathing variations during the transition to unconsciousness are related to variations in regional activity.

Two different fMRI models were estimated. The first model (breathing-fall map) included 30 image volumes (1 min) preceding transition and the subsequent 20 vol (40 s) coinciding with the observed transitory reduction in ventilation (see below in Results). The second model (breathing-recovery map) also included this 20-volume period (40 s) and the subsequent 30 vol (1 min) of breathing recovery (Fig. 2). Therefore, these fMRI models allowed us to differentially identify brain regions coupled to breathing from wakefulness to loss of consciousness and regions coupled to breathing recovery during the unconscious state.

Resulting 1st-level contrast images were carried forward to 2nd-level analyses in SPM. One-sample t-test maps were estimated for both breathing-fall and breathing-recovery models. Two-sample paired t-test maps were obtained comparing the models. A motion summary measure (mean inter-frame motion (Pujol et al., 2014)) for each participant was included as a covariate to further control potential motion effects.

Breathing is often considered a major confounding factor in fMRI, particularly when assessing functional connectivity, and diverse procedures may be applied to remove the artifactual effects (Murphy et al., 2013; Power et al., 2017). However, care should be taken to avoid removing the neural signal one is trying to detect. In our analysis of slow ventilation changes, we considered it relevant to assess the potential

influence on the results of the delayed vascular effects of breathing variations on the fMRI signal (Chang and Glover, 2009). Therefore, the results were replicated after additionally including the individual RVT time courses with a long delay in the 1st-level models. A lapse of +18 s was used as the typical time required to achieve the full vascular effects (Chang and Glover, 2009; Birn et al., 2008).

Results were considered significant when clusters formed at a threshold of $p < 0.005$ survived whole-brain family-wise error (FWE) correction ($p < 0.05$), calculated using SPM.

3. Results

3.1. Ventilation changes at loss of consciousness

Fig. 1 shows representative single-subject plots illustrating changes in ventilation associated with propofol-induced loss of consciousness. A transient reduction in ventilation (measured as respiration volume per time, RVT) was identified, with an onset approximately coinciding with the onset of fMRI signal transitional changes (i.e., the initial fMRI signal fall). This transient decrease in ventilation was notably consistent across subjects (Fig. 2). As a group, RVT measures showed values below baseline for 40 s (i.e., 20 image volumes). Interestingly, a degree of breathing synchronization across subjects (i.e., RVT oscillations detectable at the group level) was also observed prior to reduced ventilation and following recovery (Fig. 2).

Such consistent across-subject variations in ventilation were, however, discreet in terms of their effect on oxygenation and carbon dioxide measures. Oxygen saturation during the transition period showed no
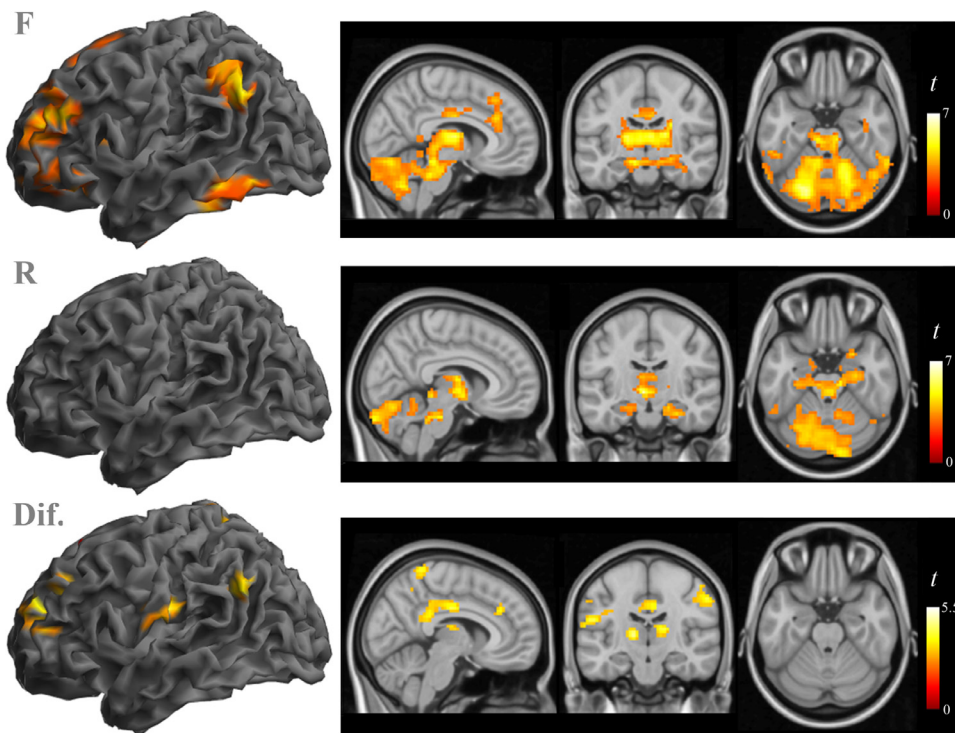
Fig. 3. Breathing-coupled brain activity. SPM maps were generated using individual breathing (RVT) time courses as regressors. The "breathing-fall map" (F, superior images) shows cortical and subcortical structures coupled to breathing from wakefulness to loss of consciousness. The "breathing recovery map" (R, middle images) shows deep brain structures coupled to breathing recovery during the unconscious state. The inferior images show the map of the differences (Dif.) between the fall in breathing and breathing recovery, which included cortical areas and the thalamus. The left hemisphere is displayed on the left side of the coronal and axial views.

net change with a ceiling effect consistently at values always of 99% or over in both baseline and transition periods. Note that the participants received a continuous administration of inhaled oxygen at 2 L/min during the experiment. The change in end-tidal carbon dioxide was also not significant, showing a mean $\pm$ SD of 34.1 $\pm$ 2.4 mmHg prior to the transitional phenomena and 33.9 $\pm$ 3.5 mmHg during transition (t = 0.3; p = 0.773).

3.2. Breathing-coupled brain activity at the transition to unconsciousness

Brain elements with fMRI signal significantly coupled to breathing from wakefulness to loss of consciousness included discrete areas in the prefrontal cortex, angular/supramarginal gyri, inferior temporal cortex, cingulate cortex, hippocampus, thalamus, brainstem tegmentum and cerebellum. Structures with fMRI signal coupled to breathing recovery were restricted to the hippocampus, brainstem tegmentum, cerebellum, amygdala and the hypothalamus/subthalamus region (Fig. 3 and Table 1). Differences between both breathing-fall and breathing-recovery maps were observed in the prefrontal cortex, angular gyrus, precuneus, cingulate cortex, supramarginal/postcentral gyri, parietal operculum and thalamus (Fig. 3 and Table 2).

To control for potential vascular effects of breathing variations on fMRI signal, the results of the differences between breathing-fall and breathing-recovery maps were replicated after adjusting the first-level (single-subject) correlation maps by the RVT time courses shifted +18 s. The analysis with and without the adjustment showed similar results (Table 3).

To further illustrate the coupling of the fMRI signal to breathing, RVT measures were plotted against fMRI signal in representative brain structures (Fig. 4). The angular gyrus showed the best coupling to RVT before and during the breathing fall. In contrast, the hypothalamus region was best coupled to RVT during breathing recovery and the brainstem showed some coupling in both phases.

As mentioned, fMRI signal in the hippocampus was significantly associated with breathing variations in both phases. Nevertheless, the affected hippocampus portion was not identical. In the breathing-fall map, the implicated area extended from the subiculum to the region of the

dentate gyrus and CA4, whilst in the breathing recovery map, it extended from the subiculum to the parahippocampal gyrus (Fig. 5). The differences between both maps were not significant. However, at a low threshold (uncorrected p < 0.05), the association between fMRI signal and breathing measures was stronger during unconsciousness in the anterior extent of the subiculum and CA1.

4. Discussion

We examined the relationships between breathing and fMRI signal changes associated with propofol-induced loss of consciousness. The analysis confirmed the study's hypothesis that a subtle, albeit consistent, reduction in ventilation coincided with the beginning of the fMRI transitional phenomenon, specifically with a general fMRI signal decline in the cerebral cortex. Such a respiratory depression was transitory and recovered during the unconscious state after 40 s in average. The mapped correlation between breathing and fMRI signal variations from wakefulness to loss of consciousness captured a combination of cortical and subcortical structures. In contrast, breathing recovery was coupled to fMRI signal in deep structures only.

We proposed that a transitory decoupling in cortico-subcortical synchrony would allow the brain to detach from waking activity and reorganize during the unconscious state and used breathing as a basic behavior to illustrate such a transition to the new order. The temporal coincidence between the beginning of the ventilation reduction and the initial fMRI signal decline observed in the synchronized cerebral cortex supports that the identified imaging changes captured the transition to unconsciousness gently induced by the hypnotic agent. Interestingly, the relatively long duration of both behavioral and imaging events further indicates that the apparently abrupt loss of consciousness may be only the initial step of a complex transitional phenomenon (Pujol et al., 2021).

The current analysis showed a notably distinctive set of brain structures coupled to decreased and recovered breathing levels. Only the brainstem tegmentum, cerebellum and hippocampus were identified in both maps. The most basic breathing control takes place in the brainstem and deep brain structures (Smith and Lee-Chiong, 2008;

Table 1
Breathing-coupled brain activity at loss of consciousness.

	Cluster size voxels (ml)	$P_{FWE\text{-}corr}$	Peak x y z	T	P
Breathing fall					
L Prefrontal Cortex	9287 (250.7)	<1e-10	−32 42 21	7.1	9e-7
R Prefrontal Cortex	"	"	34 48 12	5.0	0.00006
L Thalamus	"	"	−17 −18 9	5.6	0.00002
R Thalamus	"	"	13 −6 9	6.6	2e-6
L Inferior Temporal Cortex	"	"	−47 −39 −21	5.3	3e-5
R Inferior Temporal Cortex	"	"	64 −45 −21	4.6	0.0001
Brainstem Tegmentum	"	"	−5 −27 −21	5.0	0.00006
Cerebellum	"	"	−20 −72 −27	6.5	3e-6
L Hippocampus	"	"	−20 −21 −15	5.4	0.00002
R Hippocampus	"	"	25 −18 −12	5.0	0.00006
Posterior Cingulate Cortex	"	"	4 −12 30	4.2	0.0003
Anterior Cingulate Cortex	"	"	10 33 30	4.7	0.0001
L Supramarginal/Angular Gyri	365 (9.9)	0.0001	−53 −57 36	4.8	0.00009
R Angular Gyrus	217 (5.9)	0.005	55 −57 39	4.7	0.0001
Breathing recovery					
Brainstem Tegmentum	2876 (77.7)	<1e-10	−5 −27 −27	5.5	0.00002
Cerebellum	"	"	1 −75 −18	4.9	0.00006
L Hippocampus	"	"	−17 −21 −15	5.5	0.00002
R Hippocampus	"	"	13 −27 −12	6.1	6e-6
L Amygdala	1100 (29.7)	1e-10	−17 0 −15	5.1	0.00005
R Amygdala	"	"	16 0 −15	4.2	0.0003
Hypothalamus	"	"	−4 −6 −6	5.5	0.00002
Subthalamic Region	"	"	−8 −12 −3	8.0	2e-7

All findings correspond to positive associations (i.e., higher RVT with higher fMRI signal). $P_{FWE\text{-}corr}$, P (Family-Wise Error corrected). x y z, coordinates given in Montreal Neurological Institute space.

Table 2
Differences in breathing-coupled fMRI signal between breathing-fall and breathing-recovery maps.

	Cluster size voxels (ml)	$P_{FWE\text{-}corr}$	Peak x y z	T	P
Fall > Recovery					
L Prefrontal Cortex	275 (7.4)	0.001	−23 57 21	4.5	0.0002
L Thalamus	89 (2.4)	0.013*	−14 −18 6	4.5	0.0002
R Thalamus	51 (1.4)	0.015*	16 −18 12	4.1	0.0004
R Supramarginal/Postcentral Gyri	226 (6.1)	0.003	40 −27 36	5.2	0.00004
L Parietal Operculum	154 (4.2)	0.027	−50 −15 21	4.4	0.0002
L Angular Gyrus	62 (1.7)	0.008*	−53 −57 33	3.9	0.001
Posterior Cingulate Cortex	353 (9.5)	0.0001	7 −15 33	4.2	0.0003
Anterior Cingulate Cortex	170 (4.6)	0.017	10 33 30	5.4	0.00002
Precuneus	192 (5.2)	0.009	4 −45 69	4.6	0.0001
Fall < Recovery					
R Hippocampus	44 (1.2)	ns	19 −15 −24	3.2	0.003
L Hippocampus	65 (1.8)	ns	−8 −3 −27	2.6	0.009

$P_{FWE\text{-}corr}$, P (Family-Wise Error corrected). x y z, coordinates given in Montreal Neurological Institute space.

* Significant with small volume correction within the region of interest.

Table 3
Differences in breathing-coupled fMRI signal between breathing-fall and breathing-recovery maps adjusted by RVT +18 s.

	Non-adjusted			Adjusted by RVT +18s		
Fall > Recovery	Peak x y z	T	P	Peak x y z	T	P
Prefrontal Cortex	−23 57 21	4.5	0.0002	−26 30 30	5.0	0.00006
L Thalamus	−14 −18 6	4.5	0.0002	−17 −21 9	4.4	0.0002
R Thalamus	16 −18 12	4.1	0.0004	16 −12 12	3.7	0.001
R Supramarginal/Postcentral G.	40 −27 36	5.2	0.00004	58 −24 42	4.5	0.0002
L Parietal Operculum	−50 −15 21	4.4	0.0002	−62 −21 21	3.7	0.001
L Angular Gyrus	−53 −57 33	3.9	0.001	−53 −57 33	5.0	0.00006
Posterior Cingulate Cortex	7 −15 33	4.2	0.0003	−2 −24 39	4.2	0.0003
Anterior Cingulate Cortex	10 33 30	5.4	0.00002	13 30 30	5.7	0.00001
Precuneus	4 −45 69	4.6	0.0001	7 −42 72	5.2	0.00003

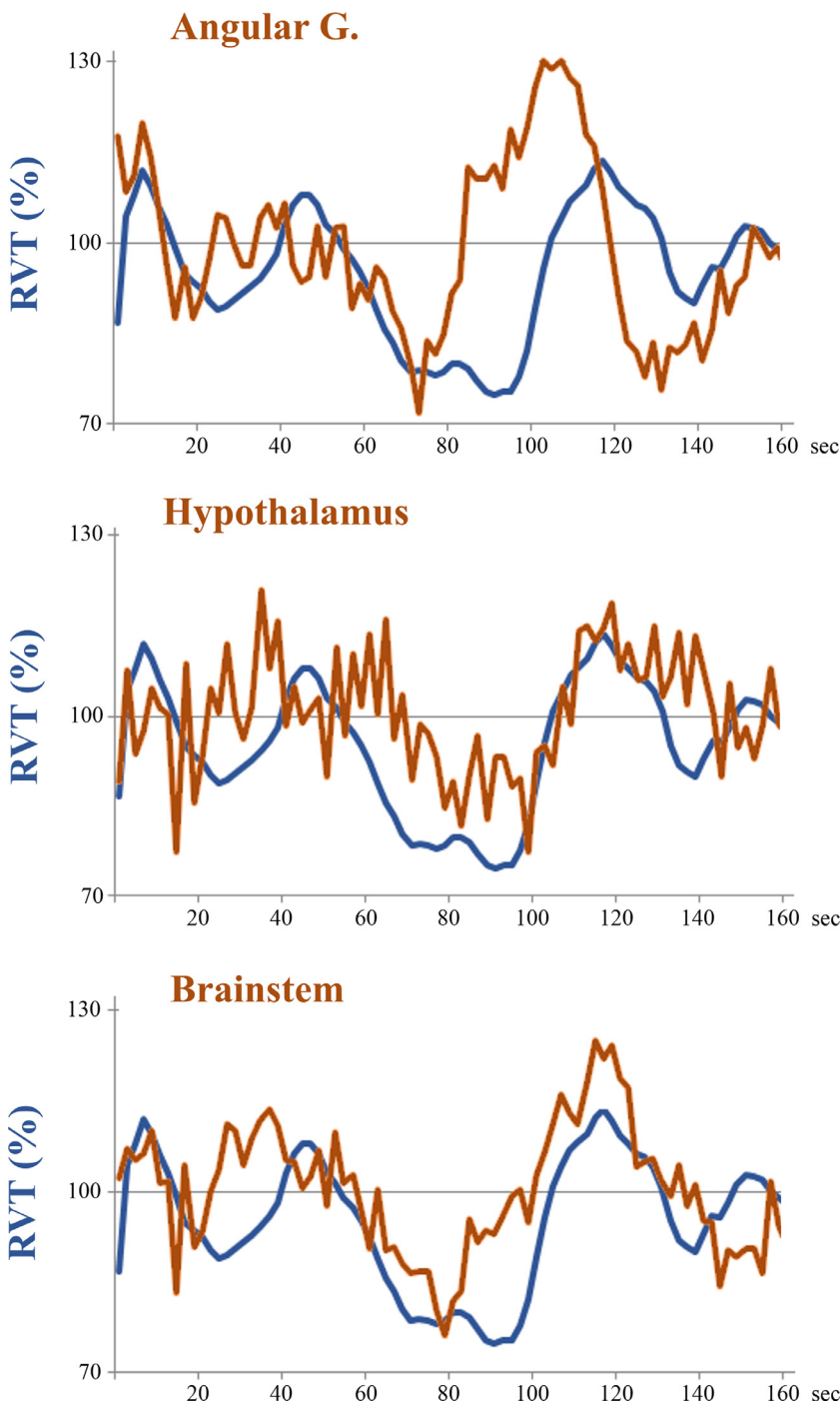x y z, coordinates given in Montreal Neurological Institute space.

Fig. 4. Group average breathing measures plotted against fMRI signal in representative brain structures.

Benarroch, 2019; Bosch et al., 2017). Therefore, it is likely that breathing variations are coupled to fMRI signal in deep brain systems in both conscious and unconscious states.

The breathing-fall map additionally included the prefrontal cortex, inferior temporal cortex, angular/supramarginal gyri, cingulate cortex and thalamus. Moreover, the postcentral gyrus and parietal operculum were identified in the difference map. All these elements may therefore potentially contribute to account for the so-called wakefulness stimulus to breathing. The transient decrease in breathing at the onset of natural or induced sleep is supposed to be, to a notable extent, the result of a sudden loss of the wakefulness drive, defined as brain activity that differentially stimulates breathing while the subject is awake (Horner, 2009; Trinder et al., 2014; Orem, 1990). Ac-

tivity in these structures may express different aspects of consciousness, and they have all been involved in either the voluntary control or conscious perception of breathing (Evans, 2010; Davenport and Vovk, 2009). The identified areas in the prefrontal cortex may play an important role in cognitive awareness (McCaig et al., 2011; Brown et al., 2019). The angular gyrus and the cingulate cortex are key elements of the default mode network, which has been consistently involved in "self-awareness" (Moll et al., 2007; Leech and Sharp, 2014; Pujol et al., 2019). As part of the sensory system, the thalamus, postcentral gyrus, parietal operculum and supramarginal gyrus each contribute to somatosensory awareness (de Haan and Dijkerman, 2020; Keller at al., 2020). Therefore, the breathing-fall map included elements of brain systems responsible for relevant components of conscious activity with
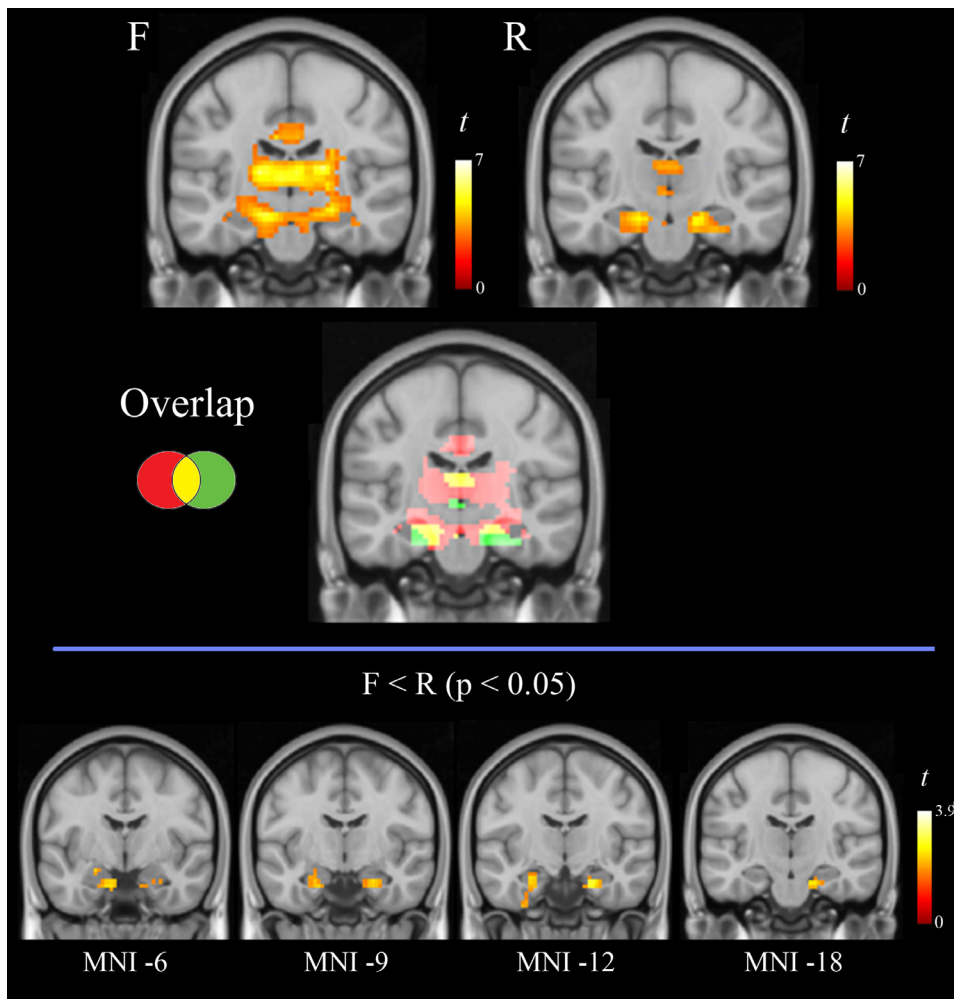
Fig. 5. Illustration of the correlation between breathing variations and fMRI signal in the hippocampus. The superior images show a coronal section of the breathing fall (F) and breathing recovery (R) maps. The middle image shows the overlap (yellow) between breathing fall (red) and breathing recovery (green) results. The inferior images show several coronal sections of the contrast "breathing fall < breathing recovery". MNI, Montreal Neurological Institute coronal coordinates in mm. The left hemisphere is displayed to the left of the images.

a potential direct or indirect influence on breathing in the waking state.

Our results also showed brain structures unique to the breathing recovery map such as the amygdala, hypothalamus and subthalamus. Although we found no significant differences when comparing both maps at this level, the finding is of interest insofar as it suggests a prominent participation of primary systems controlling instinctive and homeostatic behaviors in the modulation of breathing during unconsciousness. Activity in the amygdala and hypothalamus is typically synchronized with a range of autonomic responses including cardio-respiratory coupling, sweating and blood pressure (Masaoka et al., 2014; Fukushi et al., 2019). Notable variations in autonomic activity exist during sleep (Penzel et al., 2016; Fukushi et al., 2019). Interestingly, the hypothalamus, which has a distinctive role in the general regulation of the wake-sleep cycle (Saper et al., 2010), showed a distinctive fMRI signal dynamics at loss of consciousness (Pujol et al., 2021) and the closest coupling to breathing recovery in the current analysis (Fig. 4).

As mentioned, the hippocampus was identified in both maps. However, the hippocampal sectors associated with breathing fall and breathing recovery did not completely overlap in our analysis. This interesting observation further emphasizes that the hippocampal neural processes at work during wakefulness and unconsciousness are not identical. Indeed, although vivid experiences with emotional and physiological components may occur both in wakefulness and during natural (Dresler et al., 2014) or propofol-induced unconsciousness (Sanders et al., 2012; Radek et al., 2018) in the form of dreams, waking experiences are recorded in memory and dreams are not.

Previous imaging studies have mostly focused on identifying neural systems related to several aspects of conscious breathing based on strategies differing from the one used here, including hypernea, respiratory load, breath-hold, restricted tidal volume and hypercapnia. Although the previous work does not directly compare with our study, it jointly indicates that the major functional brain systems processing sensorimotor, limbic and cognitive activity may be linked to breathing during waking activity (e.g., Davenport and Vovk, 2009; Evans, 2010; Macey et al., 2016; Chan et al., 2018). Of special interest may be the studies illustrating how the neural correlates of spontaneous breathing differ during cognitive challenging compared with rest and show a degree of task specificity as to the brain areas implicated (Evans et al., 2009; Zhang et al., 2020).

A significant limitation of our study lies in its correlational nature, which allows for alternative interpretations. That is, although the identified brain systems may plausibly contribute to driving breathing, as suggested herein, they could also potentially express bottom-up influences of breathing on brain activity (Girin et al., 2021; Herrero et al., 2018; Heck et al., 2017), or a combination of both events. An interesting example of bottom-up relationships is the enhancement of our sense of smell during inhalation (Masaoka et al., 2014), via synchronization of brain activity to the respiratory phase (Ito et al., 2014; Nguyen-Chi et al., 2016) and enhancement of cortical rhythms specifically during a phase of the respiratory cycle (Tort et al., 2018; Masaoka et al., 2014). However, both strong odors and direct stimulation of olfactory-related brain areas produce rapid and important changes in breathing (Masaoka et al., 2014). That is, sensory system activity may drive breathing and, in turn,

brain activity rhythms may be phase-locked to the respiratory cycle. Other interesting examples of observed effects of the respiratory phase on brain activity include enhancement of pain responses (Iwabe et al., 2014) and faster recognition of fear expressions (Zelano et al., 2016) during inspiration.

We would also mention that the transitional breathing changes were pharmacologically induced. Propofol acts substantially through a GABA effect (Sahinovic et al., 2018). The GABA is the second most ubiquitous neurotransmitter present in 15%–20% of brain neurons (Buzsáki et al., 2007). As other hypnotic agents, when administered at relatively low doses and at low velocity, propofol may potentiate the neural events initiating sleep both by reducing waking cerebral cortex activity and via direct action on the brainstem arousal system (Horner, 2009; Mashour and Hudetz, 2017). Interestingly, we have recently illustrated how other hypnotics with robust GABA action, such as benzodiazepines, may alter functional connectivity in the cerebral cortex mostly affecting the primary sensory areas, which suggests that the reduction of sensory processing may be a relevant mediator of the sedative effect (Blanco-Hinojo et al., 2021). Nevertheless, propofol at higher doses and faster velocity during general anesthesia may virtually affect all neural systems (Moody et al., 2021). Therefore, although we used a slow propofol administration regime, our observations cannot be currently extrapolated to naturally induced sleep.

5. Conclusions

The study aimed to illustrate how the brain reorganizes itself to control a basic behavior when moving between states of consciousness. The adopted image analysis strategy allowed us to identify brain systems plausibly contributing to breathing modulation during wakefulness and unconsciousness. The fall in breathing from wakefulness to unconsciousness was associated with activity reduction in brain systems underlying distinct aspect of consciousness, such as cognitive awareness, self-awareness and sensory awareness. Breathing recovery during the unconscious state was coupled to deep brain structures controlling instinctive and homeostatic behaviors. All in all, in a broad sense, our results are in line with the proposals that phenomenologically contemplate consciousness as the result of the largest-scale integration of brain activity (Northoff and Lamme, 2020; Tanabe et al., 2020; Zhang et al., 2020; Pujol et al., 2021).

Declaration of Competing Interest

The authors report no financial interests or potential conflicts of interest.

Credit authorship contribution statement

Jesus Pujol: Conceptualization, Data curation, Supervision, Writing – original draft. **Laura Blanco-Hinojo:** Formal analysis, Writing – review & editing. **Héctor Ortiz:** Supervision, Conceptualization, Writing – review & editing. **Lluís Gallart:** Supervision, Conceptualization, Writing – review & editing. **Luís Moltó:** Investigation, Writing – review & editing. **Gerard Martínez-Vilavella:** Formal analysis, Writing – review & editing. **Esther Vilà:** Investigation, Writing – review & editing. **Susana Pacreu:** Investigation, Writing – review & editing. **Irina Adalid:** Investigation, Writing – review & editing. **Joan Deus:** Conceptualization, Writing – review & editing. **Víctor Pérez-Sola:** Conceptualization, Writing – review & editing. **Juan Fernández-Candil:** Supervision, Data curation, Conceptualization, Writing – review & editing.

Funding

Data and code availability statement

Data will be available via a request to the Authors with no particular restrictions, although a formal data sharing agreement will be considered.

References

Benarroch, E.E., 2019. Control of the cardiovascular and respiratory systems during sleep. Auton. Neurosci. 218, 54–63 May.

Birn, R.M., Smith, M.A., Jones, T.B., Bandettini, P.A., 2008. The respiration response function: the temporal dynamics of fMRI signal fluctuations related to changes in respiration. Neuroimage 40 (2), 644–654 Apr 1.

Blanco-Hinojo, L., Pujol, J., Macià, D., Martínez-Vilavella, G., Martín-Santos, R., Pérez–Sola, V., Deus, J., 2021. Mapping the synchronization effect of gamma-aminobutyric acid inhibition on the cerebral cortex using magnetic resonance imaging. Brain Connect 11 (5), 393–403 Jun.

Bosch, L., Fernández-Candil, J., León, A., Gambús, P.L., 2017. Influence of general anaesthesia on the brainstem. Rev. Esp. Anestesiol. Reanim. 64 (3), 157–167 Mar.

Brown, R., Lau, H., LeDoux, J.E., 2019. Understanding the higher-order approach to consciousness. Trends Cognit. Sci. 23 (9), 754–768 Sep.

Buzsáki, G., Kaila, K., Raichle, M., 2007. Inhibition and brain work. Neuron 56 (5), 771–783 Dec 6.

Chan, P.S., Cheng, C.H., Wu, Y.T., Wu, C.W., Liu, H.A., Shaw, F.Z., Liu, C.Y., Davenport, P.W., 2018. Cortical and subcortical neural correlates for respiratory sensation in response to transient inspiratory occlusions in humans. Front Physiol 9, 1804 Dec 18.

Chang, C., Glover, G.H., 2009. Relationship between respiration, end-tidal CO_2, and BOLD signals in resting-state fMRI. Neuroimage 47 (4), 1381–1393 Oct 1.

Davenport, P.W., Vovk, A., 2009. Cortical and subcortical central neural pathways in respiratory sensations. Respir. Physiol. Neurobiol. 167 (1), 72–86 May 30.

de Haan, E.H.F., Dijkerman, H.C., 2020. Somatosensation in the brain: a theoretical re-evaluation and a new model. Trends Cognit. Sci. 24 (7), 529–541 Jul.

Dresler, M., Eibl, L., Fischer, C.F., Wehrle, R., Spoormaker, V.I., Steiger, A., Czisch, M., Pawlowski, M., 2014. Volitional components of consciousness vary across wakefulness, dreaming and lucid dreaming. Front. Psychol. 4, 987 Jan 2.

Edwards B.A., White D.P. Control of the pharyngeal musculature during wakefulness and sleep: implications in normal controls and sleep apnea. Head Neck. 2011 Oct;33 Suppl 1(Suppl 1):S37–45.

Evans, K.C., Dougherty, D.D., Schmid, A.M., Scannell, E., McCallister, A., Benson, H., Dusek, J.A., Lazar, S.W., 2009. Modulation of spontaneous breathing via limbic/paralimbic-bulbar circuitry: an event-related fMRI study. Neuroimage 47 (3), 961–971 Sep.

Evans, K.C., 2010. Cortico-limbic circuitry and the airways: insights from functional neuroimaging of respiratory afferents and efferents. Biol. Psychol. 84 (1), 13–25 Apr.

Fukushi, I., Yokota, S., Okada, Y., 2019. The role of the hypothalamus in modulation of respiration. Respir. Physiol. Neurobiol. 265, 172–179 Jul.

Girin, B., Juventin, M., Garcia, S., Lefèvre, L., Amat, C., Fourcaud-Trocmé, N., Buonviso, N., 2021. The deep and slow breathing characterizing rest favors brain respiratory-drive. Sci. Rep. 11 (1), 7044 Mar 29.

Heck, D.H., McAfee, S.S., Liu, Y., Babajani-Feremi, A., Rezaie, R., Freeman, W.J., Wheless, J.W., Papanicolaou, A.C., Ruszinkó, M., Sokolov, Y., Kozma, R., 2017. Breathing as a fundamental rhythm of brain function. Front. Neural. Circuits 10, 115 Jan 12.

Herrero, J.L., Khuvis, S., Yeagle, E., Cerf, M., Mehta, A.D., 2018. Breathing above the brain stem: volitional control and attentional modulation in humans. J. Neurophysiol. 119 (1), 145–159 Jan 1.

Horner, R.L., 2009. Emerging principles and neural substrates underlying tonic sleep-state-dependent influences on respiratory motor activity. Philos. Trans. R. Soc. Lond. B Biol. Sci. 364 (1529), 2553–2564 Sep 12.

Ito, J., Roy, S., Liu, Y., Cao, Y., Fletcher, M., Lu, L., Boughter, J.D., Grün, S., Heck, D.H., 2014. Whisker barrel cortex delta oscillations and gamma power in the awake mouse are linked to respiration. Nat. Commun. 5, 3572 Apr 1.

Iwabe, T., Ozaki, I., Hashizume, A., 2014. The respiratory cycle modulates brain potentials, sympathetic activity, and subjective pain sensation induced by noxious stimulation. Neurosci. Res. 84, 47–59 Jul.

Keller, M., Pelz, H., Perlitz, V., Zweerings, J., Röcher, E., Baqapuri, H.I., Mathiak, K., 2020. Neural correlates of fluctuations in the intermediate band for heart rate and respiration are related to interoceptive perception. Psychophysiology 57 (9), e13594 Sep.

Khosla, M., Ngo, G.H., Jamison, K., Kuceyeski, A., Sabuncu, M.R., 2021. Cortical response to naturalistic stimuli is largely predictable with deep neural networks. Sci. Adv. 7 (22), eabe7547 May 28.

Leech, R., Sharp, D.J., 2014. The role of the posterior cingulate cortex in cognition and disease. Brain 137 (Pt 1), 12–32 Jan.

Macey, P.M., Ogren, J.A., Kumar, R., Harper, R.M., 2016. Functional imaging of autonomic regulation: methods and key findings. Front. Neurosci. 9, 513 Jan 26.

Masaoka, Y., Izumizaki, M., Homma, I., 2014. Where is the rhythm generator for emotional breathing? Prog. Brain Res. 209, 367–377.

Mashour, G.A., Hudetz, A.G., 2017. Bottom-up and top-down mechanisms of general anesthetics modulate different dimensions of consciousness. Front. Neural. Circuits 11, 44 Jun 20.

Mayhew, D., Mendonca, V., Murthy, B.V.S., 2019. A review of ASA physical status-historical perspectives and modern developments. Anaesthesia 74, 373–379.

McCaig, R.G., Dixon, M., Keramatian, K., Liu, I., Christoff, K., 2011. Improved modulation of rostrolateral prefrontal cortex using real-time fMRI training and meta-cognitive awareness. Neuroimage 55 (3), 1298–1305 Apr 1.

Merica, H., Fortune, R.D., 2004. State transitions between wake and sleep, and within the ultradian cycle, with focus on the link to neuronal activity. Sleep Med. Rev. 8 (6), 473–485 Dec.

Moll, J., de Oliveira-Souza, R., Garrido, G.J., Bramati, I.E., Caparelli-Daquer, E.M., Paiva, M.L., Zahn, R., Grafman, J., 2007. The self as a moral agent: linking the neural bases of social agency and moral sensitivity. Soc. Neurosci. 2 (3–4), 336–352.

Moody, O.A., Zhang, E.R., Vincent, K.F., Kato, R., Melonakos, E.D., Nehs, C.J., Solt, K., 2021. The neural circuits underlying general anesthesia and sleep. Anesth. Analg. 132 (5), 1254–1264 May 1.

Murphy, K., Birn, R.M., Bandettini, P.A., 2013. Resting-state fMRI confounds and cleanup. Neuroimage 80, 349–359 Oct 15.

Naifeh, K.H., Kamiya, J., 1981. The nature of respiratory changes associated with sleep onset. Sleep 4 (1), 49–59.

Nguyen-Chi, V., Müller, C., Wolfenstetter, T., Yanovsky, Y., Draguhn, A., Tort, A.B., Brankačk, J., 2016. Hippocampal respiration-driven rhythm distinct from theta oscillations in awake mice. J. Neurosci. 36 (1), 162–177 Jan 6.

Northoff, G., Lamme, V., 2020. Neural signs and mechanisms of consciousness: is there a potential convergence of theories of consciousness in sight? Neurosci. Biobehav. Rev. 118, 568–587 Nov.

Ogilvie, R.D., 2001. The process of falling asleep. Sleep Med. Rev. 5 (3), 247–270 Jun.

Ogilvie, R.D., Wilkinson, R.T., Allison, S, 1989 Oct. The detection of sleep onset: behavioral, physiological, and subjective convergence. Sleep 12 (5), 458–474.

Orem, J., 1990. The nature of the wakefulness stimulus for breathing. Prog. Clin. Biol. Res. 345, 23–30.

Penzel, T., Kantelhardt, J.W., Bartsch, R.P., Riedl, M., Kraemer, J.F., Wessel, N., Garcia, C., Glos, M., Fietze, I., Schöbel, C., 2016. Modulations of heart rate, ECG, and cardio-respiratory coupling observed in polysomnography. Fron. Physiol. 7, 460 Oct 25.

Poldrack, R., Mumford, J., Nichols, T., 2011. Handbook of Functional MRI Data Analysis. Cambridge University Press, Cambridge.

Power, J.D., Mitra, A., Laumann, T.O., Snyder, A.Z., Schlaggar, B.L., Petersen, S.E., 2014. Methods to detect, characterize, and remove motion artifact in resting state fMRI. Neuroimage 84, 320–341 Jan 1.

Power, J.D., Plitt, M., Laumann, T.O., Martin, A., 2017. Sources and implications of whole-brain fMRI signals in humans. Neuroimage 146, 609–625 Feb 1.

Pujol, J., Blanco-Hinojo, L., Gallart, L., Moltó, L., Martínez-Vilavella, G., Vilà, E., Pacreu, S., Adalid, I., Deus, J., Pérez-Sola, V., Fernández-Candil, J., 2021. Largest scale dissociation of brain activity at propofol-induced loss of consciousness. Sleep 44 (1), zsaa152 Jan 21.

Pujol, J., Harrison, B.J., Contreras-Rodriguez, O., Cardoner, N., 2019. The contribution of brain imaging to the understanding of psychopathy. Psychol. Med. 49 (1), 20–31 Jan.

Pujol, J., Macià, D., Blanco-Hinojo, L., Martínez-Vilavella, G., Sunyer, J., de la Torre, R., Caixàs, A., Martín-Santos, R., Deus, J., Harrison, B.J., 2014. Does motion-related brain functional connectivity reflect both artifacts and genuine neural activity? Neuroimage 101, 87–95 Nov 1.

Radek, L., Kallionpää, R.E., Karvonen, M., Scheinin, A., Maksimow, A., Långsjö, J., Kaisti, K., Vahlberg, T., Revonsuo, A., Scheinin, H., Valli, K., 2018. Dreaming and awareness during dexmedetomidine- and propofol-induced unresponsiveness. Br. J. Anaesth. 121 (1), 260–269 Jul.

Sahinovic, M.M., Struys, M.M.R.F., Absalom, A.R., 2018. Clinical pharmacokinetics and pharmacodynamics of propofol. Clin Pharmacokinet. 57 (12), 1539–1558 Dec.

Sanders, R.D., Tononi, G., Laureys, S., Sleigh, J.W., 2012. Unresponsiveness ≠ unconsciousness. Anesthesiology 116 (4), 946–959 Apr.

Saper, C.B., Fuller, P.M., Pedersen, N.P., Lu, J., Scammell, T.E., 2010. Sleep state switching. Neuron 68 (6), 1023–1042 Dec 22.

Schnider, T.W., Minto, C.F., Shafer, S.L., Gambus, P.L., Andresen, C., Goodale, D.B., Youngs, E.J., 1999. The influence of age on propofol pharmacodynamics. Anesthesiology 90 (6), 1502–1516 Jun.

Smith, D.R., Lee-Chiong, T., 2008. Respiratory physiology during sleep. Sleep Med. Clin. (3) 497–503.

Tanabe, S., Huang, Z., Zhang, J., Chen, Y., Fogel, S., Doyon, J., Wu, J., Xu, J., Zhang, J., Qin, P., Wu, X., Mao, Y., Mashour, G.A., Hudetz, A.G., Northoff, G., 2020. Altered global brain signal during physiologic, pharmacologic, and pathologic states of unconsciousness in humans and rats. Anesthesiology 132 (6), 1392–1406 Jun.

Tort, A.B.L., Brankačk, J., Draguhn, A., 2018. Respiration-entrained brain rhythms are global but often overlooked. Trends Neurosci. 41 (4), 186–197 Apr.

Trinder, J., Jordan, A.S., Nicholas, C.L., 2014. Discharge properties of upper airway motor units during wakefulness and sleep. Prog. Brain Res. 212, 59–75.

Worsnop, C., Kay, A., Pierce, R., Kim, Y., Trinder, J., 1985. Activity of respiratory pump and upper airway muscles during sleep onset. J. Appl. Physiol. 85 (3), 908–920 1998 Sep.

Zelano, C., Jiang, H., Zhou, G., Arora, N., Schuele, S., Rosenow, J., Gottfried, J.A., 2016. Nasal respiration entrains human limbic oscillations and modulates cognitive function. J. Neurosci. 36 (49), 12448–12467 Dec 7.

Zhang, J., Huang, Z., Tumati, S., Northoff, G., 2020. Rest-task modulation of fMRI-derived global signal topography is mediated by transient coactivation patterns. PLoS Biol. 18 (7), e3000733 Jul 10.